ACS APPLIED NANO MATERIALS

www.acsanm.org Article

Nanoscale Self-Assembly of Poly(3-hexylthiophene) Assisted by a Low-Molecular-Weight Gelator toward Large-Scale Fabrication of Electrically Conductive Networks

Madhubhashini Lakdusinghe, Mahsa Abbaszadeh, Satish Mishra, Dineshkumar Sengottuvelu, Rangana Wijayapala, Song Zhang, Anthony R. Benasco, Xiaodan Gu, Sarah E. Morgan, David O. Wipf, and Santanu Kundu*

Cite This: *ACS Appl. Nano Mater.* 2021, 4, 8003–8014 Read Online

ACCESS | Metrics & More | Article Recommendations | Supporting Information

ABSTRACT: Achieving self-assembly of conjugated polymers is necessary to harness their charge transport properties in various applications, including field-effect transistors, sensors, and conductive gels for biomedical applications. Although many processes have been investigated, there are still opportunities for developing new strategies that can lead to materials with improved performances. Particularly, large-scale fabrication of three-dimensional conductive networks formed by the self-assembly of conjugated polymers and low-molecular-weight gelators (LMWGs), but with conjugated polymers at much lower quantity, would be advantageous. LMWGs can be selected from an extensive library of available systems and can be directed to self-assemble in various conditions. However, the simultaneous self-assembly of LWMGs and conjugated polymers is not fully understood. Here, we report a simple pathway for the self-assembly of poly(3-hexylthiophene) (P3HT), a conjugated polymer, in chloroform in the presence of di-Fmoc-L-lysine, an LMWG. Di-Fmoc-L-lysine was selected as the LMWG because it does not have significant interactions with P3HT. P3HT and di-Fmoc-L-lysine in chloroform form gels with decreasing temperature. UV−vis spectroscopy provides an insight into the photophysical response of the gelation process, revealing the self-assembly of P3HT in the gel network. The scattering experiments further capture the self-assembly of the P3HT network. The nanofibrillar microstructure has been captured using atomic force microscopy (AFM) for the gels without and with P3HT, where both P3HT and di-Fmoc-L-lysine form nanofibers independently. Both these nanofibers coexist and intermingle, displaying conductive domains in the dried films captured by conductive AFM. The conductive nanofibers form a percolated network in the dried samples, leading to bulk electrical conductivity similar to that of pristine P3HT films. This is achieved with only 20% P3HT content and the balance insulating di-Fmoc-L-lysine molecules. Our results provide a fundamental understanding of the self-assembly of P3HT in the presence of an LMWG, resulting in a conductive nanofibrillar network. Such knowledge can readily be implemented in other conjugated polymeric systems. The approach presented here has potential applications towards fabricating conductive gels for biomedical and sensor applications and large-scale processing of thin films for optoelectronic applications.

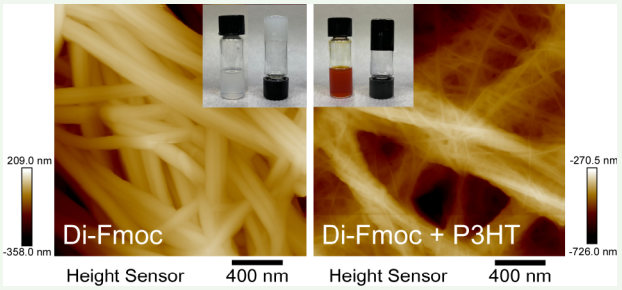

KEYWORDS: *conjugated polymer, P3HT, low-molecular-weight gelator, nanofibers, electrical conductivity, self-assembly, conductive AFM*

INTRODUCTION

The long- and short-range orders of conjugated polymers dictate the charge-transfer process in the devices fabricated from these materials.[1−5] The order of the conjugated polymers is crucial for their potential applications in optoelectronic devices, for example, organic field-effect transistors, organic light-emitting diodes, and photovoltaics, and numerous biomedical applications, including biosensors, tissue engineering, and drug delivery.[6−11] The order of conjugated polymers depends on the polymer architecture and the processing conditions utilized to process these polymers into thin films, nanofibers, gels, and other forms.[7,12−15] In most of these processing methods, the initial step involves dissolving the polymers in a suitable solvent.[13,15,16] In the solution, the conjugated polymer molecules self-assemble, particularly if the concentration is beyond the critical polymer concentration.[17−19] At sufficiently high concentrations, the formation of a liquid-crystalline phase and gelation have been observed.[12,20−25] The aggregation process and the structure

Received: May 16, 2021
Accepted: July 20, 2021
Published: July 29, 2021

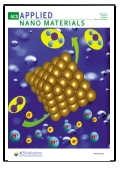

of the aggregates over different length scales depend on the polymer concentration, polymer molecular weight, regioregularity, solvent quality, and aging.[14,22,26−29] The ordered structure is then retained or modified into the final processed form, such as in thin films, nanofibers, or bulk solid.[14,30,31] Because of aromatic moieties, π-stacking is prevalent in conjugated polymers, and side-chain lamellar stacking is also possible.[17,32,33]

The ordered structure is crucial for the electronic properties of these materials, and there are many reports focusing on methods to achieve and improve the ordered structure during processing with different levels of success.[34−39] Here, we report a simple strategy for self-assembly of conjugated polymers in the solution state. Our system consists of a low-molecular-weight gelator (LMWG) and a model conjugated polymer, poly(3-hexylthiophene) (P3HT). Both LWMG and P3HT have been shown to self-assemble independently to form nanofibers in the solution state, leading to a gel-like structure. The self-assembled structure is then retained in the solid phase obtained after drying the samples. The dried gel films consist of only 20% P3HT by mass but display electrical conductivity similar to that of pristine P3HT films.

Several techniques have been pursued to control the thin-film microstructure of conjugated polymers, for example, (i) spin, dip, and blade coatings,[34−36] and (ii) drop-casting,[37] solution-shearing flow-assisted crystallization,[38] and nano-imprint lithographic techniques.[39] Starting with preformed self-assembled structures or organogels that consist of large percolating networks of self-assembled polymer nanofibrils results in better electrical conductivity in the fabricated thin film compared to the films cast from polymer solutions.[22,40−42]

P3HT, an archetype conjugated polymer, has been investigated extensively. The electrical performance of P3HT thin films is most often measured in terms of hole mobility. The hole mobility can vary from 10^{-5} to 10^{2} cm^2 V^{-1} s^{-1}, depending upon the solvent quality, assembled structure in the solution, and post-treatment methods.[42] The electrical conductivity of the thin film has also been measured, and the values are in the range of 10^{-6}−10^{-9} S cm^{-1} depending on the fabrication technique and solvents used.[43−45]

The formation of organogels at a high P3HT concentration (~10 mg mL^{-1}) in various organic solvents has been reported.[13,20,21] The variation of the nanofibrillar network structure caused by the change in solvent quality has been shown to affect the conductivity values. Dried samples obtained from various organogels display conductivities as high as ~10^{-4} Scm^{-1}.[13,20,21,40] In addition to the organogels with only P3HT, polymer gels consisting of polystyrene and P3HT have also been investigated.[46,47] In another study, the cogelation of poly(γ-benzyl-L-glutamate) (PBLG) and P3HT has been reported, where it has been shown that both polymers interact to form interconnected networks.[8] The in situ polymerization of conductive polymers in molecular gels has also been reported. For example, gels consisting of folic acid and in situ polymerized polyaniline in a water−DMSO mixture have been shown to have improved mechanical and electronic properties.[48] Different from these approaches, in our case, instead of pure P3HT, we have considered P3HT and an LMWG. These do not have significant molecular interaction and can self-assemble independently, producing a self-sustaining gel-like material. Note that the P3HT concentration used here was much lower than that necessary for the gelation of P3HT alone.

Gels formed by LMWGs, often designated as molecular gels, are widely studied materials investigated for many applications such as drug delivery, tissue engineering, and cancer treatments.[49−56] Depending on the chemical structure and their interactions with the solvents, LMWGs can self-assemble in water, organic solvents, and organic−water mixed solvents. The self-assembly process can lead to different types of nanostructures, including the nanofibrillar one.[57,58] Here, di-Fmoc-L-lysine (denoted as di-Fmoc), a peptide-based LMWG with two Fmoc moieties, has been considered. This LMWG can form both organogels and hydrogels through π-interaction between Fmoc moieties and through hydrogen bonding between the peptide groups.[57,58] The di-Fmoc molecules form long nanofibers immobilized with solvents, leading to gel-like materials.[57]

Here, gels consisting of di-Fmoc and P3HT were formed using the temperature-triggered gelation method. We have elucidated the self-assembly process of di-Fmoc and P3HT in the solution state using shear rheometry and spectroscopy experiments. The microstructure was further analyzed by X-ray scattering and the regular and conductive atomic force microscopy (AFM) techniques on the carefully dried samples. The charge-transport behavior in the dried samples was measured through electrical conductivity measurements. Our results indicate that it is possible to engineer the self-assembly of conjugated polymers for electronic applications using the molecular gels as a template. These materials have potential applications as conductive gels for biomedical and sensoring applications.[6,10,11] Furthermore, the strategy applied here can be used in the large-scale processing of thin films for optoelectronic applications.[59,60]

EXPERIMENTAL SECTION

Materials. P3HT was obtained from Rieke Metals (Lincoln, NE). Based on the information provided by Rieke Metals, P3HT has a regioregularity of 96.2% estimated from the nuclear magnetic resonance (NMR) data and a M_w of 83,000 g mol^{-1}, with a polydispersity index of 2.2 determined using gel permeation chromatography. Di-Fmoc-L-lysine (denoted as di-Fmoc herein), chloroform (>99.5%), and Fomblin Y LVAC 14/6 oil (molecular weight of 2500 g mol^{-1}) were obtained from Sigma-Aldrich. All chemicals were used as received. Interdigitated electrodes (IDEs) were obtained from Metrohm DropSens.

Preparation of Organogels. Hybrid gels consisting of di-Fmoc and P3HT were prepared by the temperature triggered method. The desired amounts of di-Fmoc and P3HT were added to chloroform, and the mixture was heated in a closed vial at 55 °C using a water bath. Intermittent brief sonication (30 s) was used to assist the dissolution of di-Fmoc and P3HT. After each sonication cycle, the vial was immediately placed in a hot water bath at 55 °C. Sonication caused cloudiness in the samples that contained di-Fmoc, and reheating at 55 °C made it transparent. When the sample contained both di-Fmoc and P3HT, the color of the sample appeared darker and cloudy after sonication. These samples were reheated until they became transparent orange. The orange color and the transparency were considered an indication of samples mostly devoid of P3HT aggregates; however, some aggregation cannot be completely avoided. The same procedure was applied for pristine P3HT solutions. The complete dissolution process took about 300 s.

Once a clear orange solution was obtained, the solution was allowed to cool down to room temperature to obtain the gel. The di-Fmoc concentration was maintained constant at 2% (w/v) or 20 mg mL^{-1} in all samples, while that of P3HT was varied. Five different P3HT concentrations were considered: 0.0025% (0.025 mg mL^{-1}), 0.1% (1 mg mL^{-1}), 0.2% (2 mg mL^{-1}), 0.3% (3 mg mL^{-1}), and 0.5% (5 mg mL^{-1}) (w/v), considering the volume of chloroform as the

https://doi.org/10.1021/acsanm.1c01294
ACS Appl. Nano Mater. 2021, 4, 8003−8014

basis. Pristine gel samples of di-Fmoc were also prepared using the same protocol. P3HT was also dissolved in chloroform at 55 °C without di-Fmoc, but this sample did not form a gel when cooled down to room temperature.

AFM, conductivity measurements, and scattering studies were conducted on dry gel samples. For these experiments, the pre-gel solution was drop-cast on a substrate of choice (Figure 1). The substrates were glass, mica, and silicon wafer and were used as received. The pre-gel solution was then placed in a chloroform-saturated chamber for 24 h for gelation and structural transformation to take place. The lid of the chamber was partially opened after 24 h. The gel layer on the substrate slowly dried in about 15 min as the solvent evaporated from the chamber, forming a smooth thin film of dry gel. The smooth sample surface facilitated the AFM measurements.

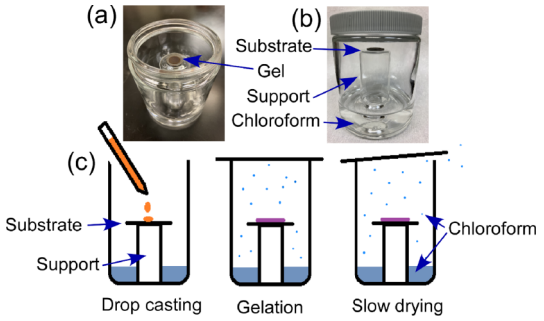

Figure 1. Images showing the (a) top and (b) front views of a thin gel layer on a mica substrate in a solvent-saturated chamber. (c) Schematics showing the sample preparation steps: drop-casting the pre-gel solution on a substrate, gel formation on the substrate in a solvent-filled chamber, and slow drying of the gel sample by partially opening the lid.

Rheological Study. The rheological investigations were conducted using a TA Instruments HR-2 Discovery rheometer equipped with a Peltier stage. A 25 mm parallel plate geometry was used. The samples were loaded in the liquid state on the bottom plate at 55 °C, and a gap of 1 mm between the top and bottom plates was maintained. A pool of liquid Fomblin (perfluoropolyether) around the plates—with the sample between the plates—was maintained to minimize chloroform evaporation. The schematic of the experimental setup is shown as an inset in Figure 2d, and an image of the setup is shown in Figure S1. Fomblin and chloroform are immiscible, and no noticeable dissolution of P3HT in Fomblin was observed.

Fourier Transform Infrared Spectroscopy. Fourier transform infrared (FTIR) spectra of the samples were collected using an attenuated total reflection (ATR) accessory in a Thermo Scientific Nicolet 6700 FTIR instrument. All spectra were collected at 4 cm^{-1} resolution by averaging over 128 scans over the range of 4000−600 cm^{-1}. P3HT solution, pristine di-Fmoc, and hybrid gel samples were placed on an ATR crystal. Samples were then dried completely before scanning.

UV−Vis Analysis. Time-lapse absorption spectra during the gelation process were collected for 24 h using a Genesys 10S UV−vis spectrophotometer. The pre-gel solution was loaded in quartz cuvettes with 1 mm path length at ∼55 °C. Cuvettes were warmed before introducing the solution to avoid sudden temperature drop of the solution, resulting in uncontrolled rapid gel formation. The data collection was started immediately. The samples were not exposed to light during the prolonged experiments.

X-ray Scattering Characterization. Grazing-incidence wide-angle X-ray scattering (GIWAXS) experiments were conducted at the School of Polymer Science and Engineering of the University of Southern Mississippi. A Xenocs Inc. Xeuss 2.0 system with an X-ray wavelength of 1.54 Å, a sample-to-detector distance of 15 cm, and an incidence angle of 0.2° was used. For these experiments, dried gel films on the silicon substrate were investigated. Samples were kept under vacuum to minimize air scattering. Diffraction images were recorded on a Pilatus 1M detector (Dectris Inc.) with an exposure time of 1 h and processed using the Nika software package in combination with WAXS tools.[61]

Atomic Force Microscopy. The AFM study was carried out using a Bruker Dimension Icon AFM instrument at the Institute for Imaging & Analytical Technologies (I^2AT) of Mississippi State University. A thin layer of the dried gel sample was prepared on the mica and glass substrates using the process described above (see Figure 1). The imaging was carried out in both ScanAsyst and tapping modes with ScanAsyst-air and NCHV probes, respectively. AFM scans were conducted with 512 × 512 pixel resolution in both modes using a 1 Hz scanning rate.

Tunneling AFM Analysis. Conductivities of dried gel samples were determined using a Bruker Dimension Icon AFM microscope at the School of Polymer Science and Engineering of the University of Southern Mississippi. The selected probe was an antimony-doped (n) silicon cantilever equipped with a platinum-coated conductive tip (radius: 25 nm). The microscope was operated in tapping mode for both conductivity mapping and current−voltage (I−V) curves. The

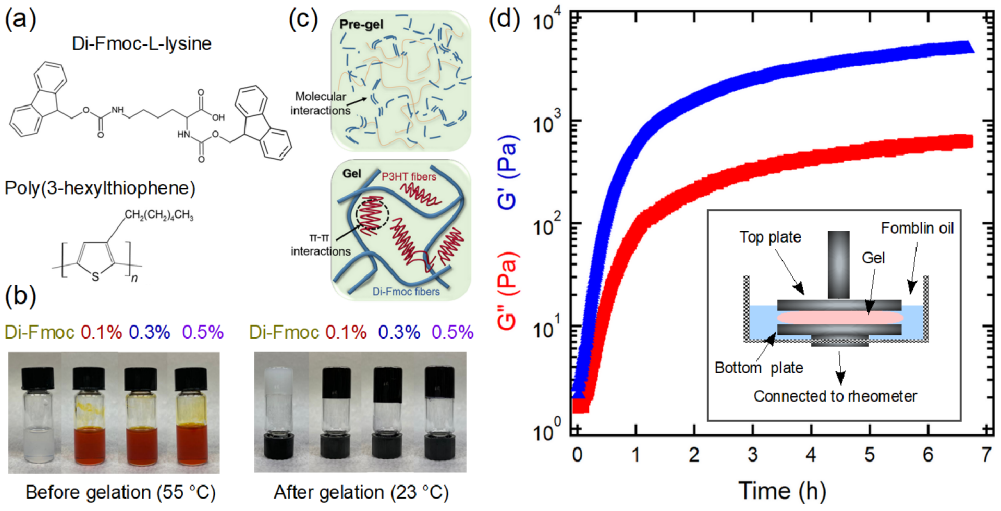

Figure 2. (a) Chemical structure of the molecular gelator di-Fmoc-L-lysine and conjugated polymer P3HT. (b) Temperature-triggered gelation of the di-Fmoc gelator with three concentrations of P3HT. (c) Schematic representation of the self-assembly process of di-Fmoc and P3HT in the gel. (d) Evolution of storage (G') and loss (G'') moduli of 0.3% gel as a function of time; the inset shows a schematic of the experimental setup.

https://doi.org/10.1021/acsanm.1c01294
ACS Appl. Nano Mater. 2021, 4, 8003−8014

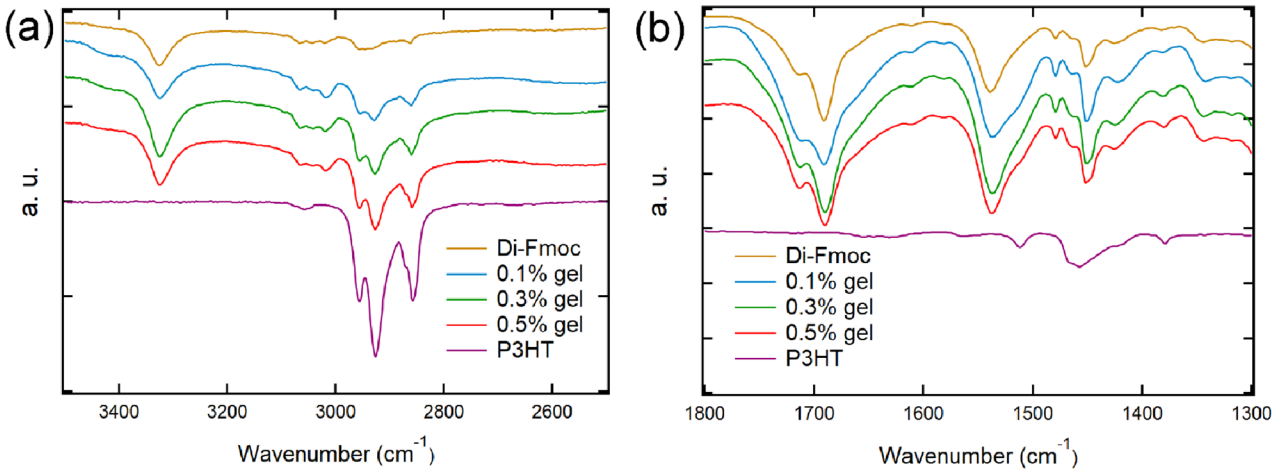

Figure 3. FTIR spectra of pristine P3HT; di-Fmoc; and 0.1%, 0.3%, and 0.5% gels in the ranges of (a) 3500−2500 and (b) 1800−1300 cm^{-1}.

sensor signal in the tunneling AFM (TUNA) scan was the electric current passing between the tip and the conductive sample under an applied DC bias voltage between 0 and 4V. Electrical contact with a standard sample chuck was established using silver colloidal paste along the edge of the substrate. The three current modes peak, contact, and TUNA are generally used in TUNA. The peak current is the instantaneous current at the maximum tip contact with the sample corresponding to the peak force. The TUNA current covers the full scan cycle (cycle average from approach to withdrawal). The peak current is higher than the TUNA current; however, the TUNA current has a higher signal-to-noise ratio.

Electrical Conductivity. The bulk conductivity of the dried gels was measured using an IDE system from Metrohm Dropsens (Spain) (Figure S2). The IDE system has two two interdigitated electrodes (bands/gaps: 10 μm, number of digits of 125 × 2) with two connection tracks made of platinum, fabricated on a glass substrate (L 22.8 × W 7.6 × H 0.7 mm). A thin dried gel layer covering the active area of the IDE was prepared by drop-casting a pre-gel solution following the same method discussed above (see Figure 1). One hundred microliters of the solution was used in every experiment to obtain uniform film thickness. The IDE was inserted in an adaptor, which was then connected to a Keithley 2450 sourcemeter via a cable connector. The bulk conductivity (σ) was obtained by dividing the cell constant of the IDE (K) by the measured resistance (R). The cell constant of the IDE was estimated as $K = \frac{2\left(\frac{S}{W}\right)^{1/3}}{\frac{L}{N}}$, where L, W, N, and S are the length, width, number of digits, and gap of separation, respectively.

RESULTS AND DISCUSSION

Gelation and Determining Gelation Kinetics Using Rheology. Gels consist of only di-Fmoc (2% (w/v)), with chloroform as the basis, and di-Fmoc (2% (w/v)) with different P3HT concentrations prepared by using the temperature-triggered method. Three P3HT concentrations of 0.1%, 0.3%, and 0.5% (w/v) with chloroform as the basis were considered. Both the gelators were dissolved in chloroform at 55 °C. For pure di-Fmoc in chloroform, a clear solution was obtained, whereas for the P3HT-containing systems, orange transparent solutions were obtained. Both pristine di-Fmoc solution and P3HT-containing di-Fmoc solutions formed gels when they were cooled to room temperature (~23 °C). The gel formation was confirmed via the vial inversion test (Figure 2b). The di-Fmoc solution formed a slightly opaque whitish gel (defined as pristine gel from here onward). On the other hand, the orange P3HT−containing solutions changed to dark magenta-brown gels, denoted as hybrid gels from here onward (Figure 2b). However, the gel formation and such color changes were not observed for the pristine P3HT solutions over the concentration range of 0.1−0.5% (w/v) considered here, even after 24 h of aging (Figure S3). The color changes in these systems have been attributed to the self-assembly of P3HT.[31] From here onwards, the gels containing 0.1%, 0.3%, and 0.5% (w/v) of P3HT and 2% di-Fmoc have been denoted as 0.1%, 0.3%, and 0.5% gels, respectively.

Both pristine and hybrid gels are thermoreversible in nature. The gel sample turned into a liquid once heated to 55 °C and became a gel again when the temperature was decreased to room temperature (Figure S4). The color change was also reversible, as the dark magenta-brown gel changed to transparent orange once in the liquid state. Upon cooling, the dark magenta-brown gel was obtained again. This process was repeatable multiple times. The thermoreversibility is related to the dissociation and reformation of the self-assembled structure caused by an increase and a decrease in temperature, respectively.

The gelation behavior was also captured using shear rheometry. Although rheometry is a common technique to capture the gelation behavior of LMWGs and the mechanical properties of the resultant gels,[32] the experiments are challenging for organogels, as the solvent can evaporate during the experiments. In our experiments, a Petri dish was attached to the bottom plate (see the inset of Figure 2d), and once the pre-gel solution at 55 °C was loaded in the parallel plate geometry, the Petri dish was filled with fluorinated oil (Fomblin Y LVAC 14/6). The oil level was maintained slightly above the edge of the top plate. This setup suppressed the solvent evaporation during the long rheological experiments (~7 h).

Figure 2d displays the evolution of the storage (G') and loss moduli (G'') as a function of time for the 0.3% gel sample obtained from the time-sweep experiment. The applied strain was 0.1% with an oscillation frequency of 1 rad/s. The initial steep increase of G' and G'' indicates a rapid gel formation. However, a crossover between G' and G'', typically defined as the gelation point,[58] could not be captured. This was likely due to the immediate onset of the gelation process as the sample was introduced to the geometry. After the initial increase, G' and G'' reached an apparent plateau, indicating that the gel network evolved to almost an equilibrium structure. However,

https://doi.org/10.1021/acsanm.1c01294
ACS Appl. Nano Mater. 2021, 4, 8003−8014

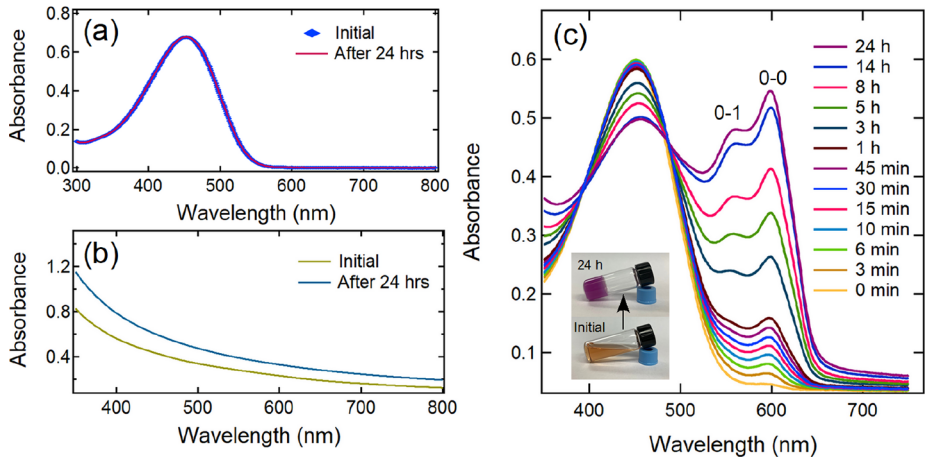

Figure 4. UV−vis profiles of (a) P3HT solution with a concentration of 0.0025% (w/v) and (b) pre-gel solution of pristine di-Fmoc and gel phase after 24 h. (c) Time-lapsed data over 24 h of gelation for a sample with 2% (w/v) of di-Fmoc and 0.0025% (w/v) of P3HT; the inset shows the initial sample image and that after 24 h. No baseline correction has been performed here.

a clear plateau had never reached, suggesting that the structure continued to evolve even after 7 h. After 5 h, 0.3% gel displayed $G' \approx 5000$ Pa and $G'' \approx 500$ Pa. Similar time-dependent behavior was observed for all gels with and without P3HT (Figure S5). All of these samples reached similar G' (3500−5500 Pa) and G'' (300−550 Pa) values after 90 min (Figure S5). Thus, the addition of P3HT does not have a strong effect on the G' and G'' values of the gels; however, it appears that P3HT-containing gels have a slightly lower modulus.

The gelation of the di-Fmoc gelator in mixed solvents has been reported earlier.[57,58] Those gels have a modulus similar to that presented here. The experimental and simulation studies show that di-Fmoc molecules form long fibrous structures with 10-100 nm diamaters and those long fibers topologically interact (entangle) to form a 3D network.[57,58] At high concentrations, P3HT also forms gels in xylene, toluene, and benzene with G' values of ∼2000 Pa for the P3HT concentration of ≈30 mg mL^{-1}.[22] In these gels, the P3HT molecules have been shown to self-assemble to form nanofibers. In addition, thermoreversible behavior has been observed in all of these gels similar to that observed here.

Although the introduction of P3HT did not change the moduli and time-dependent gelation behavior significantly, it cannot be concluded based on the rheological results whether di-Fmoc and P3HT cogelate or form a separate interpenetrated/intermingled network. Next, we investigate the structure of these gels, with and without P3HT, and attempt to elucidate the self-assembly process of di-Fmoc and P3HT molecules.

Elucidating Self-Assembly through Spectroscopic Analysis. *FTIR Spectroscopy.* FTIR spectroscopy was conducted to understand the interactions between di-Fmoc and P3HT. Here, the spectra were collected for the pristine P3HT film; dried pristine; and 0.1%, 0.3%, and 0.5% gels. As observed in Figure 3, the spectral features of di-Fmoc were prominent in dried hybrid gel films because of the higher weight fraction of di-Fmoc compared to P3HT. A few spectral regions are of interest. In the P3HT spectrum, the peak at 1450 cm^{-1} is associated with the stretching vibration of the thiophene ring, and the peak at 1515 cm^{-1} is associated with the carbon−carbon double bond stretching vibration.[46] The characteristic strong stretching vibrations of aliphatic (CH_2) bonds were also detected at 2906 cm^{-1} and 2851 cm^{-1}.[62] For the pristine di-Fmoc gel, >C═O stretching peaks at 1723 cm^{-1} for the acid carbonyl group and at 1688 cm^{-1} for the amide carbonyl were observed. Another broad peak for the −NH stretching vibration for the amide group of di-Fmoc has been detected at 3315 cm^{-1}. These amide vibration peaks are associated with the H-bonding between the carbonyl group and amine groups of adjacent gelator molecules.[48] In an earlier report on P3HT and PBLG gels, slight shifts of peaks, e.g., a shift of the 1720 cm^{-1} peak (carbonyl peak) of PBLG and the CH-stretching peak (2845−3100 cm^{-1}) of P3HT, have been detected, which are attributed to the possible interactions between two components.[8] However, in our hybrid gel samples, the spectral features of both P3HT and di-Fmoc can be found without any significant change, indicating no significant interactions between di-Fmoc and P3HT molecules.

UV−Vis Spectroscopy. Real-time UV−vis absorption spectra were collected to examine the morphological changes during the gelation process. For this experiment, the concentration of P3HT was 0.0025% (w/v), much lower than 0.1−0.5% (w/v) considered for other experiments. At higher P3HT concentrations, despite using a short, 1 mm path length, the transmission through the samples was very low and good data could not be collected. Spectra were also collected for the pristine di-Fmoc sample and P3HT solution with concentrations of 2% and 0.0025% (w/v), respectively. The di-Fmoc sample did not show any special spectral feature during the gelation process (Figure 4b). The non-gel-forming P3HT solution displayed a broad absorption peak at about 449 nm, which did not undergo any noticeable transformation over 24 h. This broad absorption peak corresponds to amorphous polymer chains;[26,31] thus, no significant self-assembly was evident for this polymer concentration.

In contrast, the UV−vis spectra for the sample of di-Fmoc and P3HT evolved during the 24 h of data collection (Figure 4c). Apart from the broad band at 449 nm, two low-energy peaks emerged at 556 and 598 nm. The intensity of these low-energy peaks continued to increase with time. These two peaks correspond to the 0−1 and 0−0 electronic transitions, respectively, and have been attributed to the aggregation of P3HT chains.[31]

The J- and H-aggregates are two types of aggregates reported for P3HT. The H-aggregates usually favor interchain

https://doi.org/10.1021/acsanm.1c01294
ACS Appl. Nano Mater. 2021, 4, 8003−8014

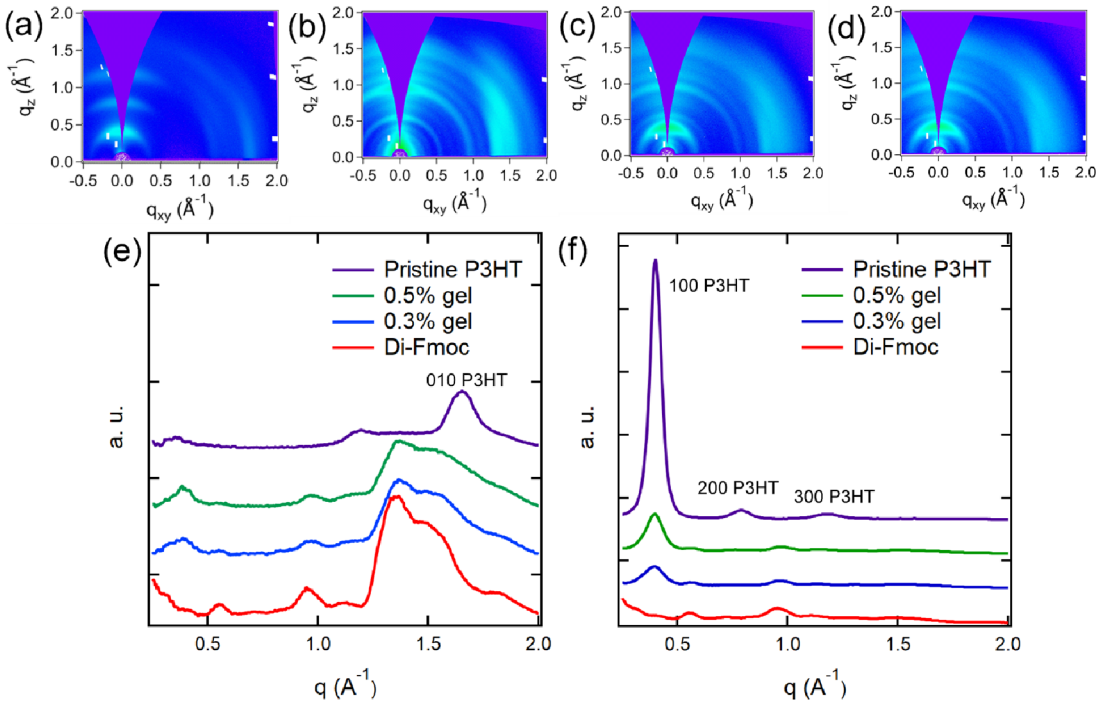

Figure 5. 2D GIWAXS of (a) pristine P3HT, (b) pristine di-Fmoc gel, (c) 0.3% gel, and (d) 0.5% gel. (e) In-plane and (f) out-of-plane 1D GIWAXS profiles of pristine P3HT, di-Fmoc, and 0.3% and 0.5% gels.

exciton coupling, whereas J-aggregates favor intrachain exciton coupling.[23,33,63] Based on the 0−0/0−1 intensity ratio, the type of aggregation can be hypothesized. Here, a higher ratio of 0−0/0−1 intensity indicates the possible prevalence of J-aggregates in comparison to H-aggregates.[63−65] Interestingly, the aggregation of P3HT occurs in these gel samples at a low concentration. In comparison, the self-assembly of pristine P3HT solution leading to nanofiber formation has been reported for much higher concentrations, such as 1−3% (w/v) (10−30 mg mL^{-1}).[15,21,31,65] We hypothesize that gelation of di-Fmoc may have increased the local concentration of P3HT, causing their aggregation. For gels with a higher P3HT concentration considered here, similar behavior can be expected.

For the P3HT concentration considered here, the aggregation kinetics, the absolute intensity of the amorphous peak and 0−0 and 0−1 transition peaks, and the ratio of 0−0/0−1 peak intensities have been found to be extremely sensitive to the experimental conditions, viz., slight variation in the sample preparation condition and room temperature and small fluctuations of P3HT and di-Fmoc weight ratios attributed to the error in measuring small P3HT mass. Because of these variations, a slight mismatch between Figure 4a−c can be observed. Note that we have not made any baseline subtraction in our data.

X-ray Scattering for Determining the Self-Assembled Structure. GIWAXS experiments were conducted to investigate the microstructure of gel samples. Figure 5a,b displays the 2D-GIWAXS data collected for pristine P3HT and pristine di-Fmoc, respectively, whereas Figure 5c,d displays that for 0.3% gel and 0.5% gel. In-plane and out-of-plane scattering profiles of pristine P3HT, di-Fmoc, and 0.3% and 0.5% gels are presented in Figure 5d,e. Similar to the gel samples, for the pristine P3HT sample, 0.3% P3HT solution in chloroform was drop-casted on a silicon wafer and was slowly dried to facilitate the self-assembly of P3HT. For this sample, the characteristic (100) peak and the higher-order (200) and (300) peaks related to the ordering along the alkyl side chains of P3HT have been observed in the out-of-plane profiles (see Figure S6 for the P3HT crystal structure). For pristine di-Fmoc samples, multiple peaks but not as sharp as those for the pristine P3HT sample were observed, corresponding to the packing of these molecules. In the 0.3% and 0.5% gel samples, the self-assembled structure of P3HT and the di-Fmoc sample were retained, evidenced by the existence of characteristic peaks from both components. At the low q region, the (100) peak of P3HT was broader and less intense along the out-of-plane direction, while the in-plane direction is less influenced. However, the peak intensity increased with the increasing concentration of P3HT (Figure 5e).

In the in-plane profiles, the 010 peak (Figure 5d) related to the $\pi-\pi$ stacking of the P3HT chains was observed in the pristine P3HT samples.[27] For the hybrid gel samples, this peak was not very prominent, as it slightly overlapped with the di-Fmoc peaks, but a weak shoulder could be noticed. The characteristic P3HT peaks in the gel samples indicate that the P3HT chains form a self-assembled structure, and such a structure has not altered significantly due to the presence of di-Fmoc. Although scattering data for dried gel samples are presented here, it is expected that somewhat similar structures are present in the gel samples, and such a structure is retained during the drying process.

Capturing Microstructure Using AFM. The nanoscale morphology of the dried gels samples was investigated using AFM. Figure 6a−c displays the fibrous structure of pristine di-Fmoc gels. As observed in Figure 6a, the fibers appeared to be thicker with diameters as high as 200 nm. These fibers are most likely a bundle of smaller diameter nanofibers, as evident from Figure 6b,c. The smallest diameter measured from the phase image is ∼80 nm. These higher-ordered features were

https://doi.org/10.1021/acsanm.1c01294
ACS Appl. Nano Mater. 2021, 4, 8003−8014

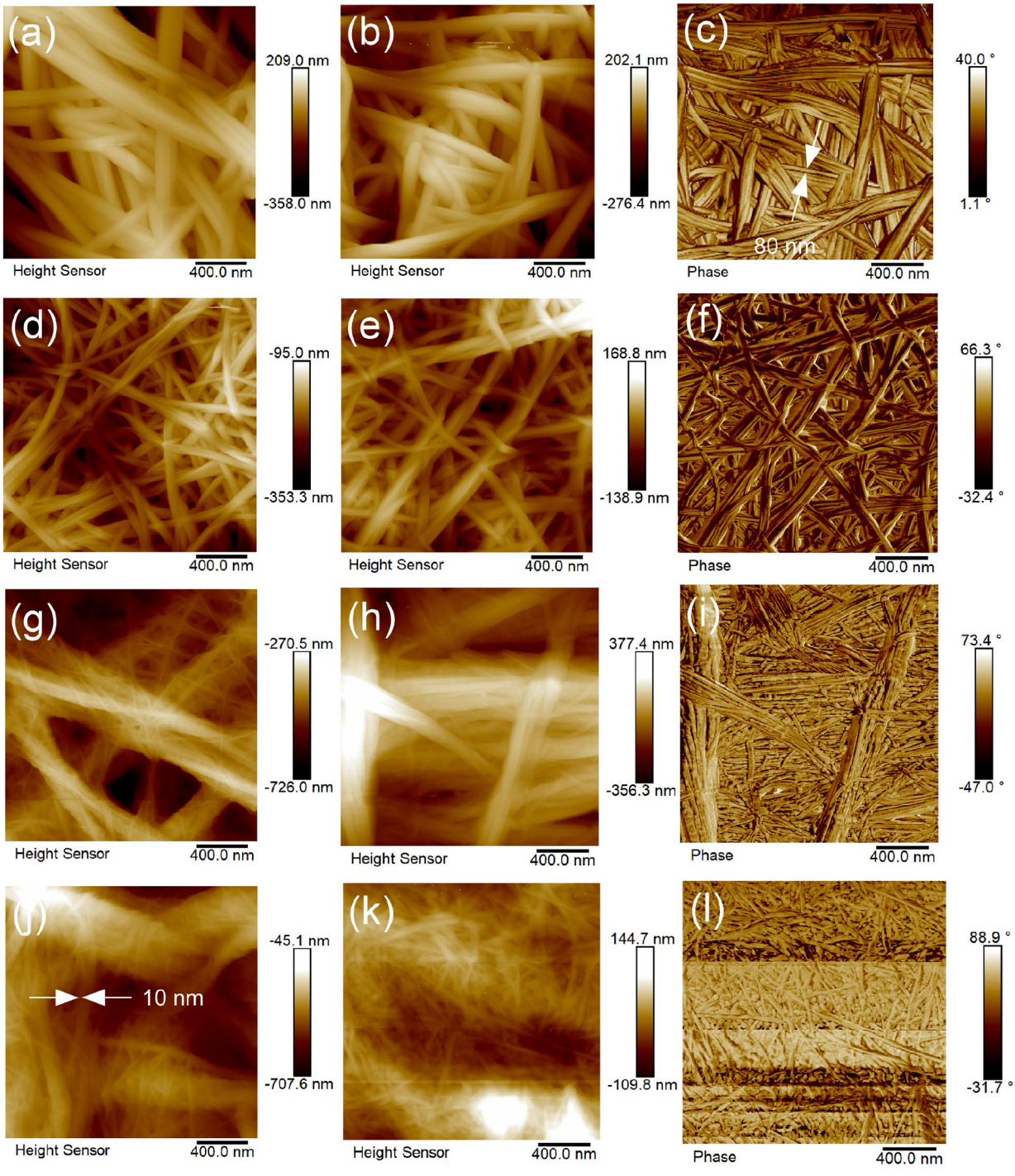

Figure 6. AFM images of dried gel samples. (a–c) Pristine di-Fmoc gel, (d–f) 0.1% gel, (g–i) 0.3% gel, and (j–l) 0.5% gel. In each row, the left image is the height image obtained by using ScanAsyst mode, whereas the center and right images are the height and phase images obtained in tapping mode.

likely formed during the drying process facilitated by favorable interactions between the fibers. These features are comparable to the results obtained from di-Fmoc gels in mixed solvents or other gels with Fmoc moieties.[25,58,66] In those studies, nanofiber diameters of 10–50 nm have been reported based on TEM and AFM measurements. AFM data also captured the bundling of those fibers.

The addition of P3HT led to a change in the microstructure of the gels (Figure 6d–l). The individual nanofibers were distinctly visible in the ScanAsyst mode, particularly for the 0.3% and 0.5% gels. The nanofiber diameter gradually decreased with increasing P3HT concentration. For the 0.3% gel, fiber diameters were in the range of 10–30 nm (Figure 6g), and for the 0.5% gel, fibers with diameters as low as 5 nm can be observed. The bundling of small fibers was also observed, but the bundles were not compact, and individual fibers could be distinguished more easily than in the pristine di-Fmoc sample.

Note that gels were prepared on various substrates such as mica, glass, and silicon wafer for the morphological character-

https://doi.org/10.1021/acsanm.1c01294
ACS Appl. Nano Mater. 2021, 4, 8003–8014

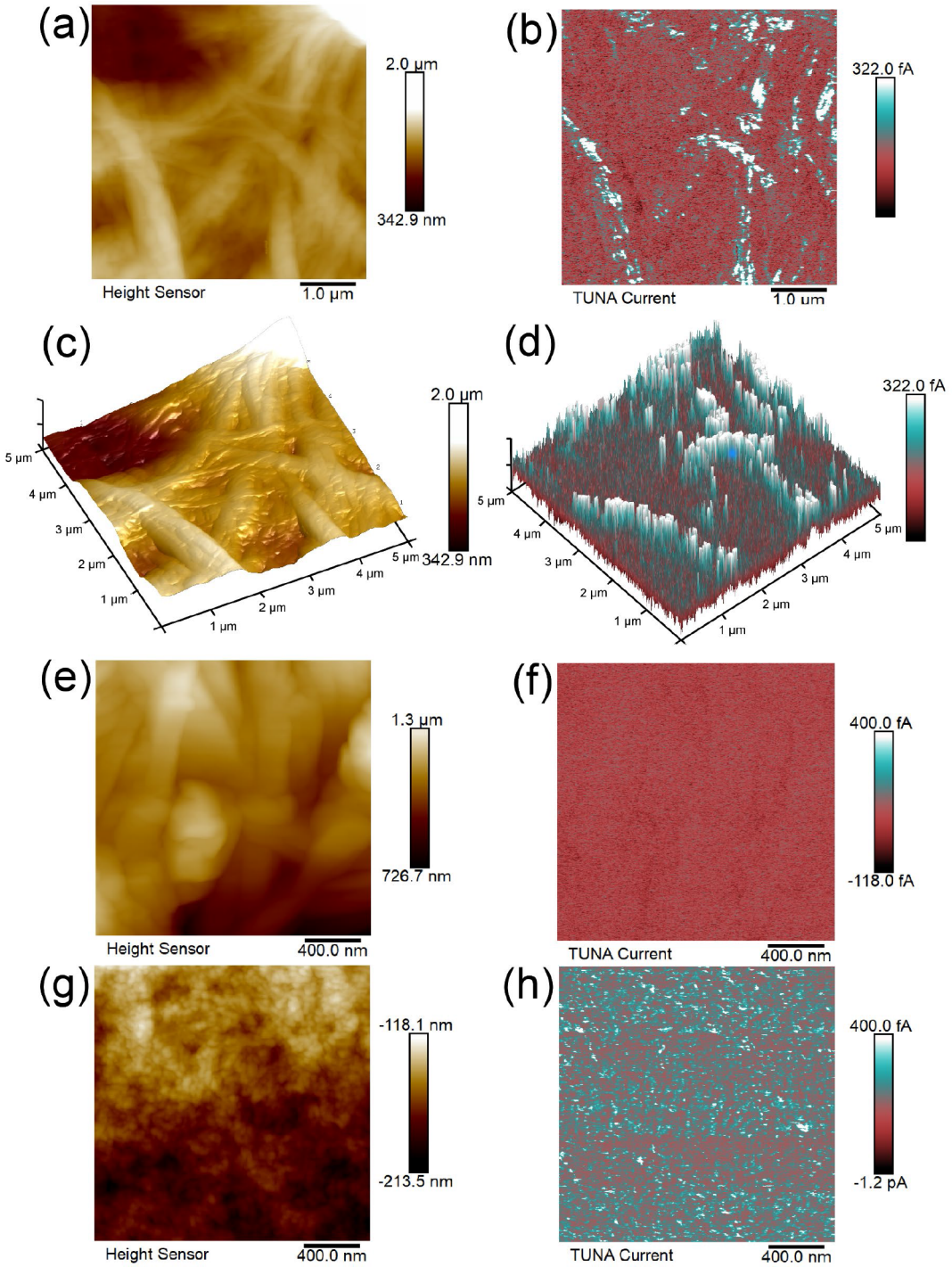

Figure 7. AFM height images and TUNA current maps. For 0.5% gel, (a) and (c) the height image and 3D height profile, respectively, and (b) and (d) the TUNA current map and 3D profile, respectively. For pristine di-Fmoc, (e) AFM height image and (f) TUNA current map. For pristine P3HT, (g) AFM height image and (h) TUNA current map. The images in Figure 7b,d were collected using a bias voltage of 2 V, whereas a bias voltage of 4 V was used for collecting the images in f,h.

izations and conductivity measurements. The AFM results do not indicate any significant differences in gel morphologies formed on different substrates.

From the AFM data, including phase images, it is not possible to differentiate Fmoc and P3HT phases/fibers, although the ratio of their volume fraction was as high as 4:1 for the 0.5% gel. Literature reports indicate that beyond a critical concentration, molecular gelators such as di-Fmoc form short, assembled structures at an early stage of gelation and that those structures continue to grow in length and width with time, forming nanofibers.[58] We hypothesize that P3HT molecules also assemble to form nanofibers. It has been shown previously that the self-assembled P3HT nanofibers can have a width of ∼10 nm,[65] similar to the di-Fmoc fibers. Because of their similar lateral dimensions, it is difficult to distinguish the di-Fmoc and P3HT nanofibers. The FTIR results (Figure 3) indicate no significant interactions between di-Fmoc and P3HT. The lack of such interactions restricted

https://doi.org/10.1021/acsanm.1c01294
ACS Appl. Nano Mater. 2021, 4, 8003−8014

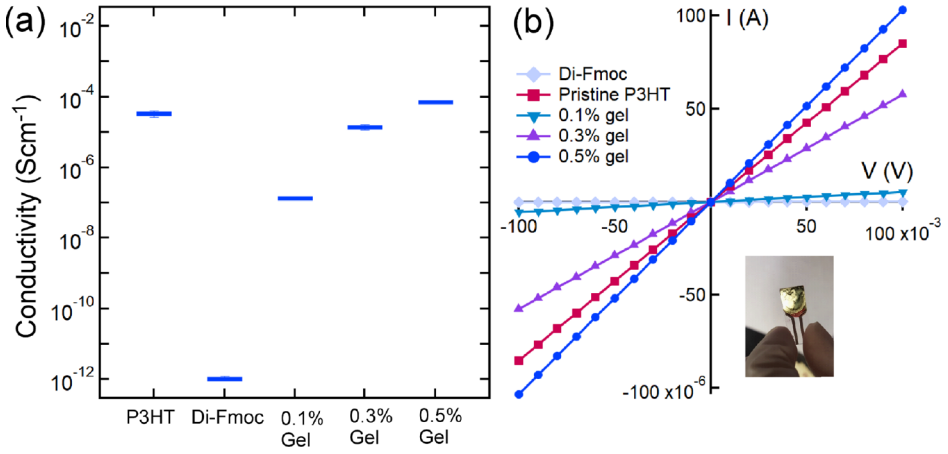

Figure 8. (a) Plot of conductivity values for pristine P3HT; di-Fmoc gel; and 0.1%, 0.3%, and 0.5% gels. (b) *I*−*V* curves for all of these samples; the inset is a thin layer of the gel sample on the IDE chip, and error bars, smaller than the symbols in some cases, represent three standard deviations.

the bundling process during drying. Here, the di-Fmoc concentration was much higher than that of P3HT, and as di-Fmoc molecules started forming nanofibers, the local concentration of P3HT increased, and the mobility of P3HT was restricted. These two phenomena promoted the self-assembly process of P3HT, leading to nanofiber formation. The self-assembly of di-Fmoc and P3HT has been schematically shown in Figure 2c.

Local Conductivity Measurements Using TUNA. TUNA, a powerful technique for nanoscale characterization of conductivity and capable of measuring ultra-low electrical currents (<1 pA), was used to capture the conductive domains in the dried gels and pristine P3HT samples (Figure 7a−h). For each sample, both the AFM image and TUNA maps were collected. Because of the larger diameter tip (25 nm) used in these experiments, the resolution of AFM images was lower than that presented in Figure 7. As expected, the pristine di-Fmoc sample did not show any signal in response to the applied bias voltage at 4 V. Therefore, the TUNA map was featureless (Figure 7f). In contrast, highly dense conductive domains were observed in the pristine P3HT sample (Figure 7h) for the same bias voltage. For the 0.5% gel sample (Figure 7a−d), the conductive domains, formed by a percolating network, were observed even at a bias voltage of 2 V. The conductive domains became more visible upon increasing the bias voltage to 4 V (Figure S7). Note that all fiber-like structures visible in Figure 7a were not conductive, and the fibers that were conductive intermingle with di-Fmoc fibers forming conductive domains. This was further evident from the 3D profiles presented in Figure 7c,d. A similar response has been observed for the 0.1% gel (Figure S8); only the number of the conductive domains was lower. These observations further support our observation that P3HT and di-Fmoc self-assemble independently into nanofibers and become intermingled.

Bulk Conductivity of Gel Samples. From the above results, it is evident that P3HT nanofibers intermingled with di-Fmoc nanofibers. If P3HT nanofibers form a percolated network, the gel samples must show bulk conductivity. The conductivity of the dried gel samples formed on an IDE chip was measured to investigate this feature. Figure 8a represents the estimated bulk conductivity values using the protocol detailed in the experimental section. The *I*−*V* curves are linear, supporting the applicability of the framework. The pristine P3HT displayed semiconductive properties having an average conductivity of ≈2.6 × 10^{-5} S cm^{-1}. Here, the result for the P3HT concentration of 0.3% is shown, but the value did not change significantly with the changing P3HT concentration. In contrast, pristine di-Fmoc gel displayed a very low conductivity value of 10^{-12} S cm^{-1}, demonstrating that this is an insulating material. For the 0.1%, 0.3%, and 0.5% gels, the conductivities were ≈1.3 × 10^{-7}, 1.4 × 10^{-5}, and 7.1 × 10^{-5} S cm^{-1}, respectively. For the 0.5% gel sample, the conductivity was slightly higher than that for pristine P3HT itself; however, it contained only 20% P3HT by weight, with the rest being an insulating material. This indicates highly ordered P3HT nanofibers and their percolated network. Because of the volatility of chloroform, we have not been able to measure the conductivity of the samples in the gel state, and in future research, less-volatile solvents will be considered. However, determining an appropriate solvent is a significant challenge. We expect that the conductivities of our hybrid gels will be comparable to those reported earlier for pristine P3HT organogels, but at lower P3HT content.

■ CONCLUSIONS

In this study, we have evaluated the self-assembly behavior of P3HT in the presence of di-Fmoc, a LMWG. This study demonstrates how a molecular gelator can assist the self-assembly of P3HT at lower concentrations compared to the pristine P3HT solution. Both di-Fmoc and P3HT dissolve well in chloroform at elevated temperatures (55 °C) for the concentrations considered here. P3HT-containing gels display color change during the gelation process, and the spectroscopic data indicate P3HT aggregation with the progression of gelation. This behavior is not observed for pristine P3HT solutions (without di-Fmoc), with concentrations similar to those considered for the gels. With decreasing temperature, the LMWGs self-assemble into nanofibers. These nanofibers are sufficiently long, thus interacting topologically in creating a three-dimensionally cross-linked network entrapping P3HT in chloroform. FTIR data indicate no significant interactions between the molecular gelator and P3HT. P3HT molecules in the interstitial space of the di-Fmoc network have high local concentrations with restricted mobility. Such conditions assist the P3HT molecules to self-assemble independently, forming nanofibrillar structures.

https://doi.org/10.1021/acsanm.1c01294
ACS Appl. Nano Mater. 2021, 4, 8003−8014

The overall gelation of P3HT-containing systems follows the similar gelation rate of only LWMGs, as the self-assembly process of P3HT does not significantly affect the gelation behavior of LWMGs. However, in the gel state, the presence of the P3HT structure slightly reduces the shear modulus. The AFM data indicate that both di-Fmoc and P3HT molecules self-assemble to form nanofibers. The GIWAXS study suggests that the presence of crystalline domains of P3HT in the dried gels and the formation of lamella structures are evident. The di-Fmoc and P3HT nanofibers intermingle, and the TUNA images of dried gels highlighted the continuous conductive pathways among the molecular gel network. The bulk electrical conductivity values increased with the increaseing concentration of P3HT, and for the 0.5% gel sample, the conductivity is slightly higher than that of the pristine P3HT sample. However, the 0.5% hybrid gel contains only 20% P3HT by weight, with the rest being an insulating material. In summary, the LMWGs enabled the self-assembly of P3HT to form nanofibers, which is difficult to achieve with P3HT alone at that concentration.

Because of the volatility of chloroform, the long-term stability of these gels can be an issue for practical applications. Future research will involve a higher boiling point solvent to improve the stability of these gels. Furthermore, finding a suitable nonhalogenated greener solvent will be beneficial for making these materials environmentally friendly. One can prepare conductive gels consisting of conjugated polymers utilizing this framework, and these gels will have potential applications in biomedical fields and sensors. Similarly, the strategy described here can be used to prepare large-scale thin films/coatings for optoelectronic applications. The presence of a stimuli-sensitive, thermoreversible molecular gelator offers additional opportunities for using these hybrid gels as active materials.

■ ASSOCIATED CONTENT

Supporting Information

The Supporting Information is available free of charge at https://pubs.acs.org/doi/10.1021/acsanm.1c01294.

An image of the rheology setup, IDE setup, aging of P3HT in chloroform without di-Fmoc, thermoreversibility of gels, rheological data for various gels, P3HT crystal structure, and conductive AFM data for 0.5% gel with 4V voltage bias and for 1% gel with 3V bias (PDF).

■ AUTHOR INFORMATION

Corresponding Author

Santanu Kundu − *Dave C. Swalm School of Chemical Engineering, Mississippi State University, Mississippi State, Mississippi 39762, United States;* orcid.org/0000-0002-0767-0512; Email: santanukundu@che.msstate.edu

Authors

Madhubhashini Lakdusinghe − *Dave C. Swalm School of Chemical Engineering, Mississippi State University, Mississippi State, Mississippi 39762, United States*

Mahsa Abbaszadeh − *Dave C. Swalm School of Chemical Engineering, Mississippi State University, Mississippi State, Mississippi 39762, United States*

Satish Mishra − *Dave C. Swalm School of Chemical Engineering, Mississippi State University, Mississippi State, Mississippi 39762, United States*

Dineshkumar Sengottuvelu − *Dave C. Swalm School of Chemical Engineering, Mississippi State University, Mississippi State, Mississippi 39762, United States*

Rangana Wijayapala − *Dave C. Swalm School of Chemical Engineering, Mississippi State University, Mississippi State, Mississippi 39762, United States*

Song Zhang − *School of Polymer Science and Engineering, University of Southern Mississippi, Hattiesburg, Mississippi 39406, United States;* orcid.org/0000-0001-9815-7046

Anthony R. Benasco − *School of Polymer Science and Engineering, University of Southern Mississippi, Hattiesburg, Mississippi 39406, United States*

Xiaodan Gu − *School of Polymer Science and Engineering, University of Southern Mississippi, Hattiesburg, Mississippi 39406, United States;* orcid.org/0000-0002-1123-3673

Sarah E. Morgan − *School of Polymer Science and Engineering, University of Southern Mississippi, Hattiesburg, Mississippi 39406, United States;* orcid.org/0000-0002-8796-9548

David O. Wipf − *Department of Chemistry, Mississippi State University, Mississippi State, Mississippi 39762, United States;* orcid.org/0000-0003-2365-1175

Complete contact information is available at: https://pubs.acs.org/10.1021/acsanm.1c01294

Author Contributions

S.K. conceived the idea, planned the experimental framework, and supervised the research. M.L. conducted the experiments. M.L. and S.K. conducted the data analysis and data interpretation. M.L. and S.K. wrote the manuscript with feedback from all authors. M.A. assisted in running the AFM experiments, S.M. assisted in running the rheology experiments, S.Z. and X.G. conducted the scattering experiments, A.R.B. and S.E.M. performed the conductive AFM experiments, D.S. assisted in NMR measurements, D.O.W. assisted in preliminary conductivity measurement, and R.W. ran initial experiments. All authors have given approval to the final version of the manuscript.

Funding

This material is based upon work supported by the National Science Foundation under Grant no. 1757220.

Notes

The authors declare no competing financial interest.

■ ACKNOWLEDGMENTS

The authors acknowledge Dr. Iwe Chu at the Institute for Imaging & Analytical Technologies (I^2AT) of Mississippi State University for helping us in AFM characterization.

■ REFERENCES

(1) Ying, L.; Huang, F.; Bazan, G. C. Regioregular Narrow-Bandgap-Conjugated Polymers for Plastic Electronics. *Nat. Commun.* **2017**, *8*, No. 14047.

(2) Ostroverkhova, O. Organic Optoelectronic Materials: Mechanisms and Applications. *Chem. Rev.* **2016**, *116*, 13279−13412.

(3) Haedler, A. T.; Kreger, K.; Issac, A.; Wittmann, B.; Kivala, M.; Hammer, N.; Köhler, J.; Schmidt, H.-W.-W.; Hildner, R. Long-Range Energy Transport in Single Supramolecular Nanofibres at Room Temperature. *Nature* **2015**, *523*, 196−199.

(4) Zhu, J.; Han, Y.; Kumar, R.; He, Y.; Hong, K.; Bonnesen, P. V.; Sumpter, B. G.; Smith, S. C.; Smith, G. S.; Ivanov, I. N.; Do, C. Controlling Molecular Ordering in Solution-State Conjugated Polymers. *Nanoscale* **2015**, *7*, 15134−15141.

(5) Lim, J. A.; Liu, F.; Ferdous, S.; Muthukumar, M.; Briseno, A. L. Polymer Semiconductor Crystals. *Mater. Today* **2010**, *13*, 14−24.
(6) Chortos, A.; Liu, J.; Bao, Z. Pursuing Prosthetic Electronic Skin. *Nat. Mater.* **2016**, *15*, 937−950.
(7) Persson, N. E.; Chu, P.-H.; McBride, M.; Grover, M.; Reichmanis, E. Nucleation, Growth, and Alignment of Poly(3-Hexylthiophene) Nanofibers for High-Performance OFETs. *Acc. Chem. Res.* **2017**, *50*, 932−942.
(8) Rosu, C.; Tassone, C. J.; Chu, P.-H.; Balding, P. L.; Gorman, A.; Hernandez, J. L.; Hawkridge, M.; Roy, A.; Negulescu, I. I.; Russo, P. S.; Reichmanis, E. Polypeptide-Assisted Organization of π-Conjugated Polymers into Responsive, Soft 3D Networks. *Chem. Mater.* **2017**, *29*, 5058−5062.
(9) Nezakati, T.; Seifalian, A.; Tan, A.; Seifalian, A. M. Conductive Polymers: Opportunities and Challenges in Biomedical Applications. *Chem. Rev.* **2018**, *118*, 6766−6843.
(10) Alegret, N.; Dominguez-Alfaro, A.; Mecerreyes, D. 3D Scaffolds Based on Conductive Polymers for Biomedical Applications. *Biomacromolecules* **2019**, *20*, 73−89.
(11) Ma, Z.; Kong, D.; Pan, L.; Bao, Z. Skin-Inspired Electronics: Emerging Semiconductor Devices and Systems. *J. Semicond.* **2020**, *41*, No. 041601.
(12) Kaur, G.; Adhikari, R.; Cass, P.; Bown, M.; Gunatillake, P. Electrically Conductive Polymers and Composites for Biomedical Applications. *RSC Adv.* **2015**, *5*, 37553−37567.
(13) Malik, S.; Jana, T.; Nandi, A. K. Thermoreversible Gelation of Regioregular Poly(3-Hexylthiophene) in Xylene. *Macromolecules* **2001**, *34*, 275−282.
(14) Huang, Y.; Cheng, H.; Han, C. C. Temperature Induced Structure Evolution of Regioregular Poly(3-Hexylthiophene) in Dilute Solution and Its Influence on Thin Film Morphology. *Macromolecules* **2010**, *43*, 10031−10037.
(15) Chang, M.-Y.-Y.; Huang, Y.-H.-H.; Han, Y.-K.-K. Aggregation, Crystallization, and Resistance Properties of Poly(3-Hexylthiophene-2,5-Diyl) Solid Films Gel-Cast from CHCl 3/p-Xylene Mixed Solvents. *Org. Electron.* **2014**, *15*, 251−259.
(16) Keum, J. K.; Xiao, K.; Ivanov, I. N.; Hong, K.; Browning, J. F.; Smith, G. S.; Shao, M.; Littrell, K. C.; Rondinone, A. J.; Andrew Payzant, E.; Chen, J.; Hensley, D. K. Solvent Quality-Induced Nucleation and Growth of Parallelepiped Nanorods in Dilute Poly(3-Hexylthiophene) (P3HT) Solution and the Impact on the Crystalline Morphology of Solution-Cast Thin Film. *CrystEngComm* **2013**, *15*, 1114−1124.
(17) Aiyar, A. R.; Hong, J.-I.; Izumi, J.; Choi, D.; Kleinhenz, N.; Reichmanis, E. Ultrasound-Induced Ordering in Poly(3-Hexylthiophene): Role of Molecular and Process Parameters on Morphology and Charge Transport. *ACS Appl. Mater. Interfaces* **2013**, *5*, 2368−2377.
(18) Wang, G.; Persson, N.; Chu, P. H.; Kleinhenz, N.; Fu, B.; Chang, M.; Deb, N.; Mao, Y.; Wang, H.; Grover, M. A.; Reichmanis, E. Microfluidic Crystal Engineering of π-Conjugated Polymers. *ACS Nano* **2015**, *9*, 8220−8230.
(19) Kleinhenz, N.; Rosu, C.; Chatterjee, S.; Chang, M.; Nayani, K.; Xue, Z.; Kim, E.; Middlebrooks, J.; Russo, P. S.; Park, J. O.; Srinivasarao, M.; Reichmanis, E. Liquid Crystalline Poly (3-Hexylthiophene) Solutions Revisited: Role Of Time-Dependent Self-Assembly. *Chem. Mater.* **2015**, *27*, 2687−2694.
(20) Newbloom, G. M.; Weigandt, K. M.; Pozzo, D. C. Electrical, Mechanical, and Structural Characterization of Self-Assembly in Poly(3-Hexylthiophene) Organogel Networks. *Macromolecules* **2012**, *45*, 3452−3462.
(21) Newbloom, G. M.; Weigandt, K. M.; Pozzo, D. C. Structure and Property Development of Poly(3-Hexylthiophene) Organogels Probed with Combined Rheology, Conductivity and Small Angle Neutron Scattering. *Soft Matter* **2012**, *8*, No. 8854.
(22) Newbloom, G. M.; De La Iglesia, P.; Pozzo, L. D. Controlled Gelation of Poly(3-Alkylthiophene)s in Bulk and in Thin-Films Using Low Volatility Solvent/Poor-Solvent Mixtures. *Soft Matter* **2014**, *10*, 8945−8954.
(23) Kao, K. Y.; Lo, S. C.; Chen, H. L.; Chen, J. H.; Chen, S. A. Gelation of a Solution of Poly(3-Hexylthiophene) Greatly Retards Its Crystallization Rate in the Subsequently Cast Film. *J. Phys. Chem. B* **2014**, *118*, 14510−14518.
(24) Chen, C.-Y.-Y.; Chan, S.-H.-H.; Li, J.-Y.-Y.; Wu, K.-H.-H.; Chen, H.-L.-L.; Chen, J.-H.-H.; Huang, W.-Y.-Y.; Chen, S.-A.-A. Formation and Thermally-Induced Disruption of Nanowhiskers in Poly(3-Hexylthiophene)/Xylene Gel Studied by Small-Angle X-Ray Scattering. *Macromolecules* **2010**, *43*, 7305−7311.
(25) Ryan, D. M.; Anderson, S. B.; Nilsson, B. L. The Influence of Side-Chain Halogenation on the Self-Assembly and Hydrogelation of Fmoc-Phenylalanine Derivatives. *Soft Matter* **2010**, *6*, 3220−3231.
(26) Scharsich, C.; Lohwasser, R. H.; Sommer, M.; Asawapirom, U.; Scherf, U.; Thelakkat, M.; Neher, D.; Köhler, A. Control of Aggregate Formation in Poly(3-Hexylthiophene) by Solvent, Molecular Weight, and Synthetic Method. *J. Polym. Sci., Part B: Polym. Phys.* **2012**, *50*, 442−453.
(27) Na, J. Y.; Kang, B.; Park, Y. D. Influence of Molecular Weight on the Solidification of a Semiconducting Polymer during Time-Controlled Spin-Coating. *J. Phys. Chem. C* **2019**, *123*, 17102−17111.
(28) Qu, S.; Ming, C.; Yao, Q.; Lu, W.; Zeng, K.; Shi, W.; Shi, X.; Uher, C.; Chen, L. Understanding the Intrinsic Carrier Transport in Highly Oriented Poly(3-Hexylthiophene): Effect of Side Chain Regioregularity. *Polymers (Basel)* **2018**, *10*, No. 815.
(29) Kline, R. J.; McGehee, M. D.; Kadnikova, E. N.; Liu, J.; Fréchet, J. M. J.; Toney, M. F. Dependence of Regioregular Poly(3-Hexylthiophene) Film Morphology and Field-Effect Mobility on Molecular Weight. *Macromolecules* **2005**, *38*, 3312−3319.
(30) Chan, K. H. K.; Yamao, T.; Kotaki, M.; Hotta, S. Unique Structural Features and Electrical Properties of Electrospun Conjugated Polymer Poly(3-Hexylthiophene) (P3HT) Fibers. *Synth. Met.* **2010**, *160*, 2587−2595.
(31) Kleinhenz, N.; Persson, N.; Xue, Z.; Chu, P. H.; Wang, G.; Yuan, Z.; McBride, M. A.; Choi, D.; Grover, M. A.; Reichmanis, E. Ordering of Poly(3-Hexylthiophene) in Solutions and Films: Effects of Fiber Length and Grain Boundaries on Anisotropy and Mobility. *Chem. Mater.* **2016**, *28*, 3905−3913.
(32) Greco, C.; Melnyk, A.; Kremer, K.; Andrienko, D.; Daoulas, K. C. Generic Model for Lamellar Self-Assembly in Conjugated Polymers: Linking Mesoscopic Morphology and Charge Transport in P3HT. *Macromolecules* **2019**, *52*, 968−981.
(33) Clark, J.; Chang, J. F.; Spano, F. C.; Friend, R. H.; Silva, C. Determining Exciton Bandwidth and Film Microstructure in Polythiophene Films Using Linear Absorption Spectroscopy. *Appl. Phys. Lett.* **2009**, *94*, No. 163306.
(34) Tiwari, S.; Takashima, W.; Nagamatsu, S.; Balasubramanian, S. K.; Prakash, R. A Comparative Study of Spin Coated and Floating Film Transfer Method Coated Poly (3-Hexylthiophene)/Poly (3-Hexylthiophene)-Nanofibers Based Field Effect Transistors. *J. Appl. Phys.* **2014**, *116*, No. 094306.
(35) Pascual-San-José, E.; Rodríguez-Martínez, X.; Adel-Abdelaleim, R.; Stella, M.; Martínez-Ferrero, E.; Campoy-Quiles, M. Blade Coated P3HT:Non-Fullerene Acceptor Solar Cells: A High-Throughput Parameter Study with a Focus on up-Scalability. *J. Mater. Chem. A* **2019**, *7*, 20369−20382.
(36) Cohen David, N.; David, Y.; Katz, N.; Milanovich, M.; Anavi, D.; Buzhor, M.; Amir, E. Electro-Conductive Fabrics Based on Dip Coating of Cotton in Poly(3-Hexylthiophene). *Polym. Adv. Technol.* **2017**, *28*, 583−589.
(37) Huq, A. F.; Ammar, A.; Al-Enizi, A. M.; Karim, A. In-Situ Orientation and Crystal Growth Kinetics of P3HT in Drop Cast P3HT:PCBM Films. *Polymer* **2017**, *113*, 200−213.
(38) Diao, Y.; Zhou, Y.; Kurosawa, T.; Shaw, L.; Wang, C.; Park, S.; Guo, Y.; Reinspach, J. A.; Gu, K.; Gu, X.; Tee, B. C. K.; Pang, C.; Yan, H.; Zhao, D.; Toney, M. F.; Mannsfeld, S. C. B.; Bao, Z. Flow-Enhanced Solution Printing of All-Polymer Solar Cells. *Nat. Commun.* **2015**, *6*, No. 7955.

https://doi.org/10.1021/acsanm.1c01294
ACS Appl. Nano Mater. 2021, 4, 8003−8014

(39) Aryal, M.; Trivedi, K.; Hu, W. W. Nano-Confinement Induced Chain Alignment in Ordered P3HT Nanostructures Defined by Nanoimprint Lithography. *ACS Nano* **2009**, *3*, 3085−3090.
(40) Sun, X.; Ren, Z.; Liu, J.; Takahashi, I.; Yan, S. Structure Evolution of Poly(3-Hexylthiophene) on Si Wafer and Poly-(Vinylphenol) Sublayer. *Langmuir* **2014**, *30*, 7585−7592.
(41) Agbolaghi, S.; Zenoozi, S. A Comprehensive Review on Poly(3-Alkylthiophene)-Based Crystalline Structures, Protocols and Electronic Applications. *Org. Electron.* **2017**, *51*, 362−403.
(42) Emrick, T.; Pentzer, E. Nanoscale Assembly into Extended and Continuous Structures and Hybrid Materials. *NPG Asia Mater.* **2013**, *5*, e43−e43.
(43) Skrypnychuk, V.; Boulanger, N.; Yu, V.; Hilke, M.; Mannsfeld, S. C. B.; Toney, M. F.; Barbero, D. R. Barbero. Enhanced Vertical Charge Transport in a Semiconducting P3ht Thin Film on Single Layer Graphene. *Adv. Funct. Mater.* **2015**, *25*, 664−670.
(44) Osaka, M.; Benten, H.; Lee, L. T.; Ohkita, H.; Ito, S. Development of Highly Conductive Nanodomains in Poly(3-Hexylthiophene) Films Studied by Conductive Atomic Force Microscopy. *Polymer (Guildf)* **2013**, *54*, 3443−3447.
(45) Obrzut, J.; Page, K. A. Electrical Conductivity and Relaxation in Poly(3-Hexylthiophene). *Phys. Rev. B* **2009**, *80*, No. 195211.
(46) Samanta, K.; Guenet, J. M.; Malik, S. Intermingled Network of Syndiotactic Polystyrene/Poly(3-Hexylthiophene). *Macromolecules* **2019**, *52*, 8569−8576.
(47) Higashihara, T.; Takahashi, A.; Tajima, S.; Jin, S.; Rho, Y.; Ree, M.; Ueda, M. Synthesis of Block Copolymers Consisting of Poly (3-Hexylthiophene) and Polystyrene Segments through Ionic Interaction and Their Self-Assembly Behavior. *Polym. J.* **2010**, *42*, 43−50.
(48) Chakraborty, P.; Bairi, P.; Mondal, S.; Nandi, A. K. Co-Assembled Conductive Hydrogel of N -Fluorenylmethoxycarbonyl Phenylalanine with Polyaniline. *J. Phys. Chem. B* **2014**, *118*, 13969−13980.
(49) Ohsedo, Y.; Saruhashi, K.; Watanabe, H.; Miyamoto, N. Synthesis of an Electronically Conductive Hydrogel from a Hydrogelator and a Conducting Polymer. *New J. Chem.* **2017**, *41*, 9602−9606.
(50) Babu, S. S.; Praveen, V. K.; Ajayaghosh, A. Functional π-Gelators and Their Applications. *Chem. Rev.* **2014**, *114*, 1973−2129.
(51) Zhang, L.; Wang, X.; Wang, T.; Liu, M. Tuning Soft Nanostructures in Self-Assembled Supramolecular Gels: From Morphology Control to Morphology-Dependent Functions. *Small* **2015**, *11*, 1025−1038.
(52) Sang, Y.; Liu, M. Nanoarchitectonics through Supramolecular Gelation: Formation and Switching of Diverse Nanostructures. *Mol. Syst. Des. Eng.* **2019**, *4*, 11−28.
(53) Fang, W.; Zhang, Y.; Wu, J.; Liu, C.; Zhu, H.; Tu, T. Recent Advances in Supramolecular Gels and Catalysis. *Chem. - Asian J.* **2018**, *13*, 712−729.
(54) Su, W.; Yin, J.; Wang, R.; Shi, M.; Liu, P.; Qin, Z.; Xing, R.; Jiao, T. Self-Assembled Natural Biomacromolecular Fluorescent Hydrogels with Tunable Red Edge Effects. *Colloids Surf., A* **2021**, *612*, No. 125993.
(55) Zhu, J.; Zhang, X.; Qin, Z.; Zhang, L.; Ye, Y.; Cao, M.; Gao, L.; Jiao, T. Preparation of PdNPs Doped Chitosan-Based Composite Hydrogels as Highly Efficient Catalysts for Reduction of 4-Nitrophenol. *Colloids Surf., A* **2021**, *611*, No. 125889.
(56) Feng, Y.; Yin, J.; Liu, S.; Wang, Y.; Li, B.; Jiao, T. Facile Synthesis of Ag/Pd Nanoparticle - Loaded Poly(Ethylene Imine) Composite Hydrogels with Highly Efficient Catalytic Reduction of 4-Nitrophenol. *ACS Omega* **2020**, *5*, 3725−3733.
(57) Hashemnejad, S. M.; Kundu, S. Probing Gelation and Rheological Behavior of a Self-Assembled Molecular Gel. *Langmuir* **2017**, *33*, 7769−7779.
(58) Hashemnejad, S. M.; Huda, M. M.; Rai, N.; Kundu, S. Molecular Insights into Gelation of Di-Fmoc-l-Lysine in Organic Solvent-Water Mixtures. *ACS Omega* **2017**, *2*, 1864−1874.
(59) Richard, M.; Al-Ajaji, A.; Ren, S.; Foti, A.; Tran, J.; Frigoli, M.; Gusarov, B.; Bonnassieux, Y.; Caurel, E. G.; Bulkin, P.; Ossikovski, R.; Yassar, A. Large-Scale Patterning of π-Conjugated Materials by Meniscus Guided Coating Methods. *Adv. Colloid Interface Sci.* **2020**, *275*, No. 102080.
(60) Zhao, P.; Tang, Q.; Zhao, X.; Tong, Y.; Liu, Y. Highly Stable and Flexible Transparent Conductive Polymer Electrode Patterns for Large-Scale Organic Transistors. *J. Colloid Interface Sci.* **2018**, *520*, 58−63.
(61) Ilavsky, J. Nika: Software for Two-Dimensional Data Reduction. *J. Appl. Crystallogr.* **2012**, *45*, 324−328.
(62) Kalonga, G. Characterization and Optimization of Poly (3-Hexylthiophene-2, 5- Diyl) (P3HT) and [6, 6] Phenyl-C61-Butyric Acid Methyl Ester (PCBM) Blends for Optical Absorption. *J. Chem. Eng. Mater. Sci.* **2013**, *4*, 93−102.
(63) Spano, F. C.; Silva, C. H- and J-Aggregate Behavior in Polymeric Semiconductors. *Annu. Rev. Phys. Chem.* **2014**, *65*, 477−500.
(64) Niles, E. T.; Roehling, J. D.; Yamagata, H.; Wise, A. J.; Spano, F. C.; Moulé, A. J.; Grey, J. K. J-Aggregate Behavior in Poly-3-Hexylthiophene Nanofibers. *J. Phys. Chem. Lett.* **2012**, *3*, 259−263.
(65) Baghgar, M.; Labastide, J. A.; Bokel, F.; Hayward, R. C.; Barnes, M. D. Effect of Polymer Chain Folding on the Transition from H- to J-Aggregate Behavior in P3HT Nanofibers. *J. Phys. Chem. C* **2014**, *118*, 2229−2235.
(66) Chen, L.; Raeburn, J.; Sutton, S.; Spiller, D. G.; Williams, J.; Sharp, J. S.; Griffiths, P. C.; Heenan, R. K.; King, S. M.; Paul, A.; Furzeland, S.; Atkins, D.; Adams, D. J. Tuneable Mechanical Properties in Low Molecular Weight Gels. *Soft Matter* **2011**, *7*, 9721−9727.

https://doi.org/10.1021/acsanm.1c01294
ACS Appl. Nano Mater. 2021, 4, 8003−8014